Heliyon 10 (2024) e37702

Contents lists available at ScienceDirect

Heliyon

journal homepage: www.cell.com/heliyon

Research article

Interactions of memantine and rivastigmine with graphene oxide nanocarrier and beta-amyloid protein using molecular docking and in-silico methods

Fateme Davoudi [a,b], Nasrin Shadjou [a,*], Mahdieh Darroudi [c]

[a] Department of Nanotechnology, Faculty of Chemistry, Urmia University, Urmia, Iran
[b] Institute of Nanotechnology, Urmia University, Urmia, Iran
[c] Pharmaceutical Analysis Research Center, Tabriz University of Medical Science, Tabriz, Iran

ARTICLE INFO

Keywords:
Molecular docking
Nanocarriers
Alzheimer
Memantine
Rivastigmine
In silico

ABSTRACT

Alzheimer's disease is characterized by the accumulation of beta-amyloid plaques and neurofibrillary tangles. Effective therapeutic strategies involve inhibiting the formation of beta-amyloid aggregates and destabilizing existing ones. A significant challenge in current treatments is the inability of therapeutic agents to cross the blood-brain barrier, a limitation addressed by employing drug nanocarriers. This study investigates the interactions between memantine, rivastigmine, beta-amyloid structures, and graphene oxide nanocarriers using molecular docking and in silico methods. The goal is to enhance drug development through cost-effective and efficient computational techniques. Results indicate that the binding energies for memantine-beta-amyloid and rivastigmine-beta-amyloid complexes are −9.03 kcal/mol and −7.81 kcal/mol, respectively, suggesting superior stability for the memantine-beta-amyloid complex. The electrostatic energies are −1.91 kcal/mol for memantine and −0.81 kcal/mol for rivastigmine, further supporting the greater stability of the memantine complex. Additionally, memantine's interaction with graphene oxide results in more negative adsorption energy (−92.47 kJ/mol) compared to rivastigmine (−86.36 kJ/mol), indicating a stronger binding affinity. The charge transfer (Q) values are −0.41 kJ/mol for memantine and −0.33 kJ/mol for rivastigmine. The negative enthalpy (ΔH) of −85.71 kJ/mol and Gibbs free energy (ΔG) of −41.52 kJ/mol for the memantine-graphene oxide interaction suggest a spontaneous process. Both memantine and rivastigmine display similar electronic properties, but memantine shows a more effective interaction with graphene oxide, likely due to its amine functional group and spatial configuration. The adsorption energy analysis confirms that memantine forms a more stable complex with graphene oxide than rivastigmine.

1. Introduction

In the field of medical science, there is a preference for medications with specific targeting, high performance, and minimal side effects. In silico methods offer a cost-effective approach for developing drugs to treat brain-nerve diseases like Alzheimer's, reducing potential damage effectively [1]. Traditional Alzheimer's therapies face challenges in crossing the blood-brain barrier (BBB), while

* Corresponding author.
E-mail address: n.shadjou@urmia.ac.ir (N. Shadjou).

https://doi.org/10.1016/j.heliyon.2024.e37702
Received 22 May 2024; Received in revised form 30 August 2024; Accepted 9 September 2024
Available online 10 September 2024

functionalized graphene does not have this limitation. Alzheimer's, the leading cause of dementia, is characterized by memory loss, behavioral changes, impaired cognitive function, and severe depression. It was originally identified by Alois Alzheimer in 1906 after two decades of research. Although the precise cause remains unknown, potential factors including free radicals, cholinergic defects, and the accumulation of *beta*-amyloid and tau proteins have been identified by researchers. The amyloid precursor protein, essential for nerve cell growth and repair, is a key player in Alzheimer's disease and is located at the end of presynaptic axons as a membrane protein. As it deteriorates, damaged amyloid precursor protein transforms into *beta*-amyloid fragments, causing nerve cell damage and cognitive decline, ultimately leading to Alzheimer's disease. The number of amino acids at the cleavage site of the *beta*-amyloid protein can influence the formation of amyloid plaques, with *beta*-amyloid, containing forty-two amino acids, being particularly prone to plaque formation [2–5].

Currently, medications such as donepezil, galantamine, rivastigmine, and memantine are commonly prescribed to alleviate symptoms and slow disease progression [6]. Rivastigmine (Fig. S1), a reversible, long-acting, non-competitive acetylcholinesterase carbamate inhibitor, is utilized to ameliorate symptoms in the mild to moderate stages of Alzheimer's disease [7]. Its mechanism involves halting the degradation of acetylcholine, thereby impeding disease advancement and safeguarding cholinergic neurons from further damage [8].

Memantine (Fig. S2) is a non-competitive antagonist for N-methyl-D-aspartate (NMDA) receptors that is used for moderate to severe Alzheimer's disease. It prevents excitotoxic neuronal cell death without disrupting physiological synaptic activity. Memantine can increase synaptic transmission in muscarinic acetylcholine receptors and further increase the proliferation and production of mature neurons in the hippocampus, thus reducing Alzheimer's symptoms [9].

This computer software is commonly used to predict the interaction between a ligand and a receptor, such as a protein or enzyme, and to comprehend the binding mechanisms involved [10]. They are also valuable for the virtual screening of extensive compound libraries in order to identify potential hit compounds for drug discovery [11]. Molecular docking seeks to predict the top binding conformations or poses of a ligand against the target of interest, and scoring functions are used to assess the strength of the ligand-receptor interactions [12]. Moreover, molecular docking has a crucial role in the computer-aided drug design process, assisting in lead identification, optimization, and the development of new drug candidates.

Advancements in nanotechnology have made a significant impact on nanomedical research in the clinical sciences. This has led to the emergence of innovative nanodevices and nano systems that depend on the precise design and integration of functional nanomaterials [13]. One notable development is the production of nanocarriers, which are colloidal systems utilized for drug delivery and typically have a particle size of less than 1000 nm [14]. These carriers effectively encase the drug and have the ability to traverse cell membranes and biological barriers owing to their small dimensions and extensive contact surface area [15]. This enables them to convey drugs through areas with numerous restrictions [16].

Nanocarriers offer various advantages, including safeguarding drugs from degradation, reducing interactions with the biological environment, improving drug absorption into target tissues, and managing the distribution of the drug within the body. Furthermore, nanoparticles offer several improvements over traditional drug delivery systems, such as increased drug stability in systemic circulation, resulting in a longer half-life, sustained drug release, and minimized side effects. Additionally, their biodegradable and biocompatible nature implies that their metabolic by-products can be easily excreted from the body. These advancements hold great promise in enhancing drug packaging, delivery, and targeting efficacy in the domain of nanomedicine [17–20].

In recent years, there has been significant interest in graphene oxide (single-layer sheet of graphite oxide) structure [21–29]. Graphene oxide is predominantly used in the fields of sensors and drug delivery [30]. There are many types of oxygen species and bonds with carbon in the graphene oxide layer, such as epoxy, hydroxyl, carbonyl, and carboxylic groups. With a large number of functional groups, graphene oxide can interact with many chemical groups and can be easily modified to enhance its functions and generate new properties [31].

Nanomedicines designed by docking methods can be used for drug delivery with minimal toxicity [32]. In this study, the intermolecular interactions of Alzheimer's drugs (memantine and rivastigmine) with *beta*-amyloid protein and graphene oxide nanocarrier were investigated using molecular docking and DFT study [33].

2. Material and methods

Gaussian 09, Gauss View 06, Autodock 4.2, and Vinadock software were employed to predict the interactions between ligands and receptors, assisting in understanding the binding mechanisms involved.

In the molecular docking method, computer software such as Gaussian 09, Gauss View 06, Autodock 4.2, and Vina dock 1.1.2 were used. Gaussian and Gauss View software was used to draw and optimize the molecular structure of the drugs [34,35]. Autodock, and Vinadock were used for molecular docking [36,37]. Lig Plot 2.2 and Discovery Studio 2016 software were used to display interactions [38]. To perform the docking method, the genetic algorithm available in Auto-dock software was used. For this purpose, Autodock 4.2 software was installed on an 8-core computer running windows.

2.1. Docking of two drugs and beta-amyloid

Memantine's molecular structure was optimized using Gaussian software, while the *beta*-amyloid protein file was obtained from the PDB (Protein Information Bank) site with the PDB code 3lpi. The protein strand A was used for further study and selected as the receptor The pdbqt files of memantine and rivastigmine were imported, and used for molecular docking to find the best binding site of drugs and *beta*-amyloid protein. Vina dock program was used for molecular docking. In this study, 'binding sites' refer to specific

regions on the *beta*-amyloid protein targeted during docking simulations. 'Conformers' denote the ligands memantine and rivastigmine's various spatial arrangements or poses as they interact with these sites. Multiple conformers allow us to capture the ligand's flexibility and identify each site's most stable binding orientation. The initial blind docking procedure was first employed to screen the protein surface comprehensively. This was followed by targeted docking at specific sites, utilizing additional conformers to enhance the precision of the interaction analysis.

The initial study focused on conducting molecular docking simulations involving memantine and *beta*-amyloid using 20 conformers within a 126*126*126 Å grid box. Subsequently, specific docking was carried out at individual sites, producing a comprehensive dataset. To maintain accuracy, instances where the grid box covered multiple adjacent sites resulted in a single docking process.

For memantine, the first grid box encompassed sites 1, 2, and 3, with dimensions of 50*49*52 Å. The second grid box covered sites 4, 5, 6, 7, and 8 within a 50*49*51 Å space. The third grid box was dedicated to the ninth site, measuring 49*51*52 Å. The fourth grid box, measuring 52*53*49 Å, housed sites 10 and 11. The fifth grid box, with dimensions of 51*52*53 Å, included sites 12 to 17. The sixth grid box, measuring 51*49*50 Å, comprised sites 18 and 19. Finally, the seventh grid box, measuring 49*49*49 Å, corresponded to the final site, site 20.

During the molecular docking process of rivastigmine and *beta*-amyloid, blind docking was first carried out using 20 conformers within a 126*126*126 Å grid box. Specific docking was then conducted at each site using another 20 conformers, resulting in a dataset. To optimize efficiency, for closely located sites covered by the same grid box, docking was performed only once. The initial grid box covered sites 1, 2, 3, and 4 with a dimension of 50 *50*50 Å. Subsequently, a second grid box was allocated specifically for site 5 with dimensions of 50*51*49, followed by a third grid box which included sites 6 and 7 with dimensions of 49 *51*52 Å. The fourth grid box, sized at 50 *51*52 Å, was assigned to site 4, and the fifth grid box, with dimensions of 49*52*50 Å, encompassed sites 9 and 10. Similarly, the sixth to thirteenth grid boxes each contained a single site, with dimensions of 50*50 *51 Å, and finally, the fourteenth grid box covered sites 19 and 20 with dimensions of 50 *51*53 Å.

2.2. Interaction of rivastigmine and memantine with graphene oxide nanosheet

In this section, the investigation focused on studying the interactions of rivastigmine and memantine with graphene oxide nanosheet. Due to the large size of graphene oxide and the complexity of its structure, quantum calculations were carried out for specific dimensions of the graphene oxide sheets. The optimized arrangements of rivastigmine, memantine, and graphene oxide nano sheet are presented in Fig. S3.

2.2.1. DFT computational method

Density functional theory was employed to assess the electronic and structural characteristics of rivastigmine, memantine, and graphene oxide nanosheet, utilizing quantum calculations at the B97D level with the 6-31+G* basis set [39,40]. The graphene oxide nanosheet used in this study measured approximately 100 Å × 100 Å, with a thickness of 1.2 Å.

3. Results and discussions

3.1. Modeling the structure of graphene oxide and rivastigmine and memantine

The initial molecular layouts of rivastigmine, memantine, and graphene oxide sheet were generated and then fine-tuned using the B97D level and 6-31+G* basis set in the gas phase. It is important to highlight that the two-dimensional structure of graphene oxide plays a crucial role in dictating the charge and spatial distribution of the HOMO and LUMO orbitals.

3.2. Interaction of rivastigmine and memantine with graphene oxide nanosheet

To find the most stable state, the interaction between drugs and a graphene oxide nanosheet was evaluated to determine the best position of the molecules relative to each other in terms of energy absorption using current equation: $\Delta E_{adsorption} = E_{complex} - (E_{graphene\ oxide} + E_{drug})$. The interaction of rivastigmine and memantine with the graphene oxide sheet was examined using parameters such as electric dipole moment and thermodynamic properties in the gas phase. The calculated thermodynamic properties include the adsorption energy (ΔE), enthalpy (ΔH), and Gibbs free energy (ΔG). These properties offer insights into the stability and spontaneity of the interactions.

3.3. Molecular docking of memantine with beta-amyloid

The all data related to the molecular docking of memantine and *beta*-amyloid using Autodock tools software are as Table 1:

The Autodock software was used to calculate the binding data for *beta*-amyloid docking with memantine. Analysis the Autodock calculations in Table 1 reveals that the state 1 has the most favorable intramolecular (−9.33 kcal/mol), and van der Waals, hydrogen bond interactions (−7.42 kcal/mol), resulting in the lowest binding energy (−9.03 kcal/mol). This suggests that state 1 is the most stable binding conformations of the complex memantine-*beta*-amyloid. After that, the second state with binding energy of −7.34 kcal/mol is stable.

Also, Table S.1, Tab. S.2, and Fig. 1(a and b) summarize general and different interactions of memantine with amino acids in the *beta*-amyloid structure using Discovery Studio software. It has been shown that among the seven docking modes, the largest number

Table 1
Autodock software calculation data for *beta*-amyloid docking with memantine. The unit of all data is kcal/mol.

Site number	Binding -energy	Ligand-efficeiency	Inhib -costant	Intermol -energy	vdw_hb_desolve_energy	Electrostatic-energy	total_internal	Torsional-energy	Unbound-energy	clRMS	refRMS
blind	−8.75	−0.63	386.64	−9.05	−7.12	−1.93	0.08	0.3	0.08	0.0	46.5
1	−9.03	−0.64	239.62	−9.33	−7.42	−1.91	0.1	0.3	0.1	0.01	46.51
2	−7.34	−0.52	4.2	−7.63	−6.1	−1.53	0.1	0.3	0.1	0.05	31.76
3	−6.95	−0.5	8.05	−7.25	−6.04	−1.21	0.1	0.3	0.1	0.06	40.2
4	−6.79	−0.48	10.6	−7.09	−6.66	−0.43	0.1	0.3	0.1	0.03	52.85
5	−6.49	−0.46	17.52	−6.79	−4.74	−2.05	0.1	0.3	0.1	0.0	47.69
6	−6.24	−0.45	26.72	−6.54	−4.83	−1.7	0.1	0.3	0.1	0.0	45.81
7	−6.17	−0.44	29.94	−6.47	−4.35	−2.12	0.1	0.3	0.1	0.0	23.77

and types of interactions are related to the first state and then the second state, which confirms the stability of these two states compared to the others. The most important principle in docking is to find ligands with the highest conformation in the lowest binding energy. Ligands that have favorable levels of interaction, hydrogen bonding, and protein inhibition are suitable for further investigations [41–50].

In the first state, memantine exhibits hydrophobic interactions with the amino acids Trp250, Leu249, Val352, Glu351, and Tyr251, contributing to its enhanced stability. In the secondary state, memantine interacts with the amino acids Asn153, Pro149, and Ser147 within the *beta*-amyloid structure. The greater number of hydrophobic interactions in the first state may indeed contribute to the enhanced stability of memantine compared to the second state (Fig. 2A and B).

Hydrogen bonds are relatively weak but forming more hydrogen bonds is beneficial for composition as they have a longer lifespan than hydrophobic bonds and can be considered stronger. Amino acids can easily form hydrogen bonds due to their COOH and NH_2 groups. Memantine, with its cage-like structure and only one amino group (NH_2), primarily interacts with its surroundings through hydrogen bonds. According to the data in Table S1 and Table S2, memantine forms hydrogen bonds with leucine (Leu222), glutamine (Gln73), proline (Pro152), valine (Val154), and isoleucine (ILE148) amino acids. In the first state, memantine acts as the donor hydrogen and forms a hydrogen bond with glutamine as the acceptor, with a bond length of 3.04 A°. In the second state, memantine forms hydrogen bonds with proline (Pro152), valine (Val154) and isoleucine (ILE148), with bond lengths of 2.81 A°, 3.13 A°, and 3.15 A°, respectively. It can be concluded that proline has the strongest hydrogen bond among the three amino acids due to its shorter bond length. Additionally, in the first state, valine, lysine, and proline have alkyl-alkyl interactions, while in the second state, glycine has van der Waals interaction and proline has two alkyl-alkyl interactions. Also, the electrostatic interactions between the ligand and the protein (Fig. S4) can indeed stabilize the composition. The electrostatic energy amounts mentioned in Table 1 (−1.91 kcal/mol for the first state and −1.53 kcal/mol for the second state) confirm that state 1 is more stable than state 2.

3.4. Molecular docking of rivastigmine with beta-amyloid

Table 2 shows the binding energy, intramolecular energy, van der Waals, hydrogen bonding, solvent binding and electrostatic energy of *beta*-amyloid and rivastigmine interaction using Autodock tools. The binding energy between rivastigmine and beta-amyloid was found to be lower in state 1 (−7.81 kcal/mol) and state 4 (−7.72 kcal/mol) compared to the other states, indicating that these states are more stable.

According to the results from Table 2, the total energy of the interactions between the *beta*-amyloid amino acids and rivastigmine structure in state 1 is −8.49 kcal/mol, while in state 4 it is −8.33 kcal/mol. This indicates that the first state is partially more stable than the fourth state due to the lower energy level. Fig. 3(A and B) also shows various interactions, such as hydrogen bonds and van der Waals forces, between the *beta*-amyloid amino acids and rivastigmine structure.

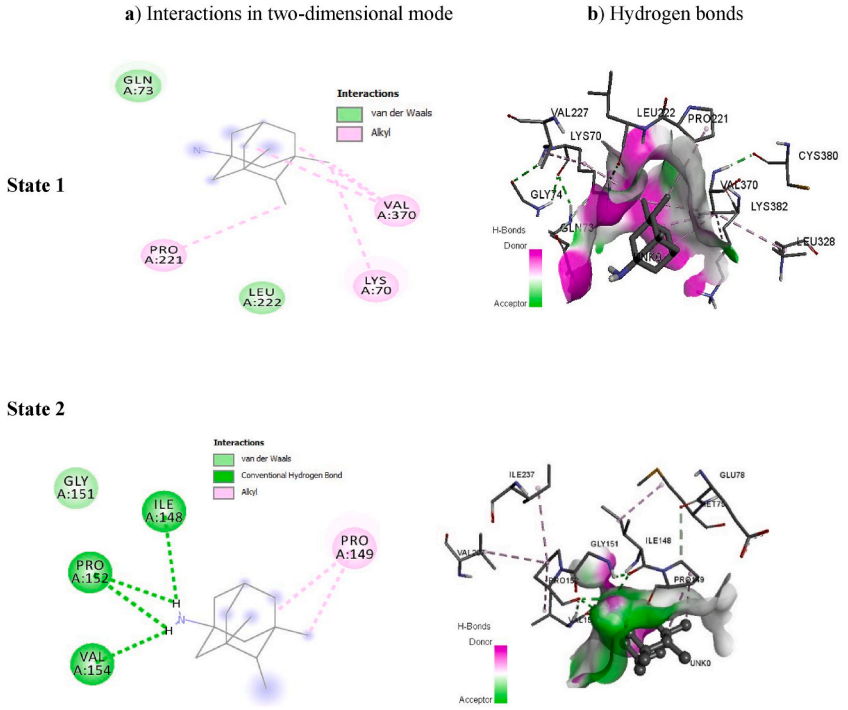

Fig. 1. The interaction of *beta*-amyloid with memantine in two more stable states. a) the two-dimensional representation of main interactions and b) the three-dimensional representation of hydrogen bond.

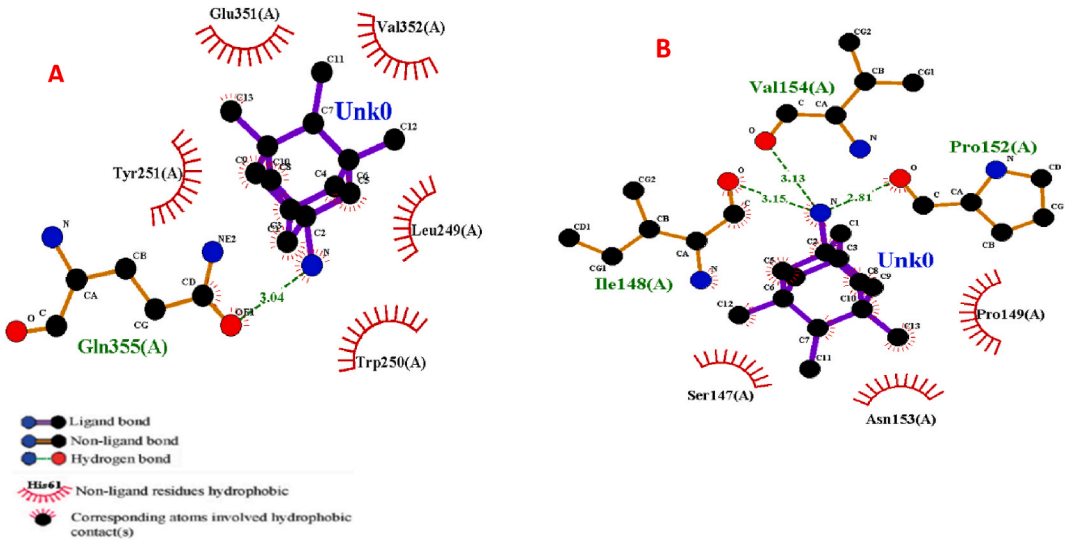

Fig. 2. A, B) Hydrogen bonds and hydrophobic interactions between *beta*-amyloid and memantine in two more stable states 1 and 2 using Lig Plot software. Semicircles and brown arcs indicate hydrophobic interactions of drugs with amino acids of *beta*-amyloid. The green dotted lines represent hydrogen bonds and the numbers on the green lines represent their bond lengths in angstroms.

In state 1, the rivastigmine structure forms hydrogen bonds with lysine (Lys70) and arginine (Arg368). The hydrogen bonds formed by arginine, utilizing its two NH_2 and one NH groups, display greater strength compared to those formed by lysine, which has an additional NH_2 group. Based on the data shown in Fig. 5, it is clear that the hydrogen bond length for arginine in state 1 is 2.89 Å, whereas for lysine, it is 2.96 Å, indicating a stronger hydrogen bond for arginine compared to lysine. In state 4, there is a hydrogen interaction between glutamic acid (Glu371) and rivastigmine with a bond length of 2.95 Å. However, it is evident that the number of hydrogen interactions in the first state is higher than that in the fourth state, implying greater stability in the first state. This supports the ratio of the binding energy between these two states (Figs. 3 and 4).

Based on Fig. 4(A and B) and Fig. S6, as well as Table S3, it is observed that rivastigmine, which contains an aromatic ring in its structure, engages in aromatic interactions with certain amino acids within the *beta*-amyloid structure. In the initial state, lysine forms a pi-sigma interaction, whereas proline and arginine exhibit a pi-alkyl interaction with the aromatic ring of rivastigmine. However, in the fourth structure, only the amino acid Lys70 interacts with the aromatic ring through a pi-carbon interaction. According to Fig. 4 and Table S3, Table S4 in the state 1, which is the most stable structure, the largest number of hydrophobic interactions takes place. The amino acids that have a hydrophobic interaction with rivastigmine in the first state are:

Val370, Glu371, Pro221, Leu222, Phe220, Tyr75, Ala218, Ser71, Gly217, Glu400, Gly219, Pro369, Gly72.

And in the fourth state are:

Gly219, Glu400, Ser71, Arg368, Pro369, Val370, Pro221, Lys70, Leu222, Phe220, Ala218.

It should be mentioned that the most type of interactions between rivastigmine and *beta*-amyloid is hydrophobic interactions. As previously mentioned, these interactions share similarities with hydrogen interactions in terms of electrostatic forces. As illustrated in Table 2, the electrostatic energy for the first state is −0.81, whereas for the fourth state it is −0.89 kcal/mol. This indicates that the electrostatic interaction in the fourth state is more stabilizing than in the first structure. Despite the increase in binding energy for the first structure due to additional hydrophobic, hydrogen, and aromatic interactions, it is generally accepted that the first state is the most stable, as indicated in Figs. S6 and S7.

3.5. General properties of rivastigmine and memantine drug interactions with graphene oxide

This study exploring the influence of various factors like local and general properties, as well as thermodynamic properties on the structural and electronic characteristics of molecules [51]. The focus of the research was on analyzing the electronic properties of graphene oxide nanosheet, as well as investigating the activity, stability, and reactivity of the drug-graphene oxide complex formed with rivastigmine and memantine. The calculation and summary of molecular orbital, energy gap, chemical hardness, chemical potential, and electron affinity of the molecules were presented in Table S.5.

According to the calculations, the energy gap of rivastigmine and memantine is 5.79 and 5.75 eV, respectively. The values of the energy gap show that rivastigmine and memantine are almost similar in terms of energy and the lower amount belongs to memantine, so it is expected that the reactivity of these two drugs is almost equal and a little better for memantine. The molecular orbital distribution of graphene oxide with rivastigmine and memantine can be seen in Fig. S8.

As we know, the amount of energy exchanged in the process of increasing an electron to a single gaseous atom in the ground state is called electron-wanting energy [52]. Also, the hardness (η) shows the resistance of the molecule to charge transfer, which is equal to

Table 2
Calculation data of Autodock software for docking *beta*-amyloid with rivastigmine. The unit of all data is kcal/mol.

Site number	Binding -energy	Ligand-efficeiency	Inhib -costant	Intermol -energy	vdw_hb_desolve_energy	Electrostatic-energy	total_internal	Torsional-energy	Unbound-energy	clRMS	refRMS
blind	−7.18	−0.4	5.46	−8.67	−7.49	−1.18	−0.48	−1.49	−0.48	0.0	45.66
1	−7.81	−0.43	1.89	−9.3	−8.49	−0.81	−0.42	1.49	−0.42	0.0	44.78
2	−5.81	−0.32	55.1	−7.3	−6.54	−0.76	−0.63	1.49	−0.63	0.0	43.94
3	−5.27	−0.29	136.58	−6.76	−5.88	−0.88	−0.49	1.49	−0.49	0.0	37.05
4	−7.72	−0.43	2.19	−9.21	−8.33	−0.89	−0.52	1.49	−0.52	0.0	44.73
5	−5.01	−0.28	212.5	−6.5	−5.71	−0.8	−0.59	1.49	−0.59	0.0	45.79
6	−4.71	−0.26	351.3	−6.2	−5.07	−1.13	−0.62	1.49	−0.62	0.0	17.16
7	−5.03	−0.28	205.46	−6.52	−5.39	−1.13	−0.63	1.49	−0.63	0.0	31.16
8	−5.43	−0.3	103.85	−6.93	−6.05	−0.88	−0.58	1.49	−0.58	0.0	37.63
9	−4.92	−0.27	248.04	−6.41	−6.01	−0.4	−0.61	1.49	−0.61	0.0	56.17
10	−5.4	−0.3	110.37	−6.89	−5.57	−1.32	−0.49	1.49	−0.49	0.0	55.28
11	−5.03	−0.28	207.01	−6.52	−5.58	−0.94	−0.59	1.49	−0.59	0.0	26.49
12	−5.26	−0.29	139.83	−6.75	−5.91	−0.84	−0.36	1.49	−0.36	0.0	26.66
13	−5.6	−0.31	78.78	−7.09	−6.72	−0.37	−0.33	1.49	−0.33	0.0	31.98
14	−6.35	−0.35	22.29	−7.74	−6.9	−0.94	−0.62	1.49	−0.62	0.0	51.33
blind	−7.18	−0.4	5.46	−8.67	−7.49	−1.18	−0.48	−1.49	−0.48	0.0	45.66

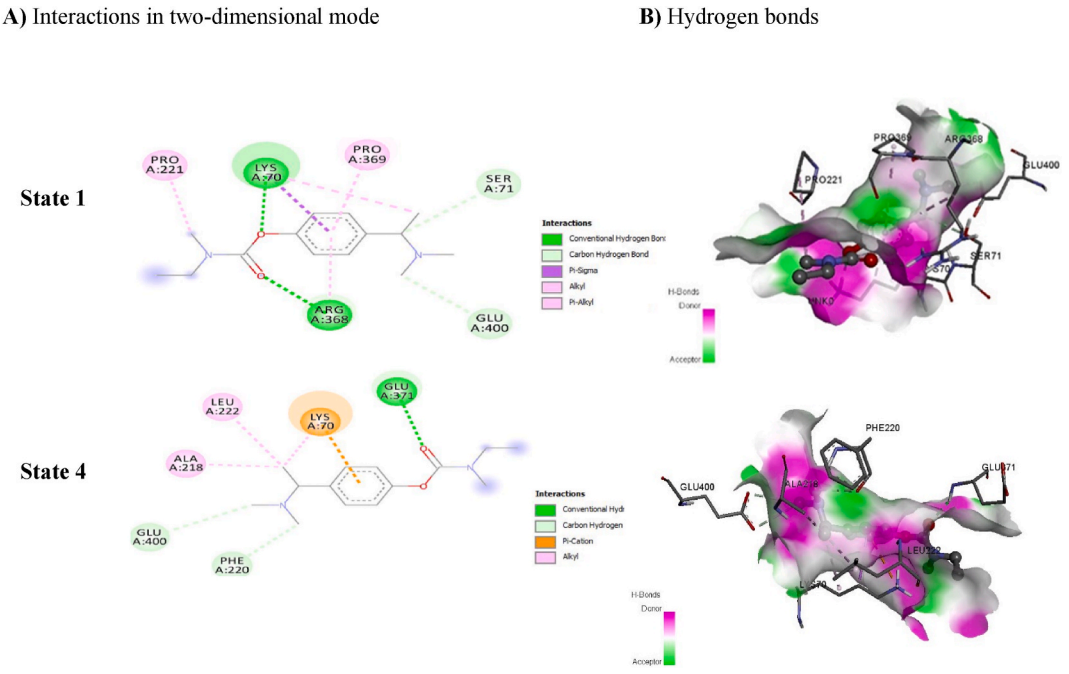

Fig. 3. The interaction of *beta*-amyloid with rivastigmine in two more stable states. **A**) the two-dimensional representation of main interactions and **B**) the three-dimensional representation of hydrogen bond.

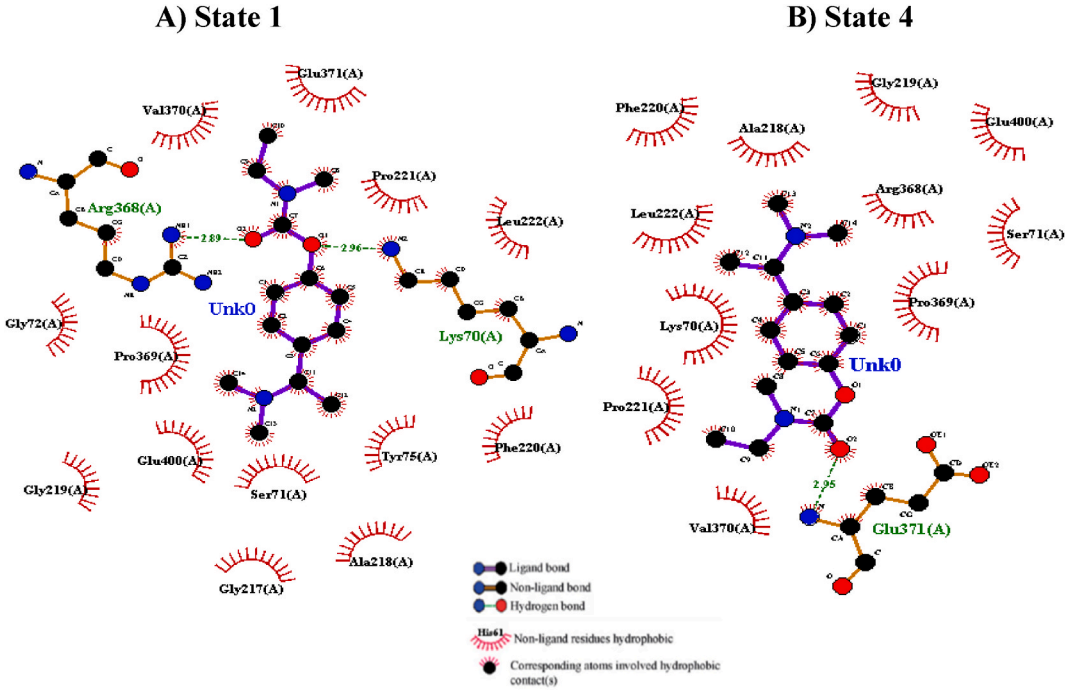

Fig. 4. (**A, B**) The interactions of the two more stable states of rivastigmine with *beta*-amyloid amino acids with Lig Plot, respectively.

half of the energy gap and is defined as equation (2) [53,54]:

$$\eta = 1/2(E_{LUMO} - E_{HOMO}) \quad \text{Eq (2)}$$

as we know the greater the energy gap between the HOMO and LUMO orbitals, the greater the chemical hardness, and also the softer

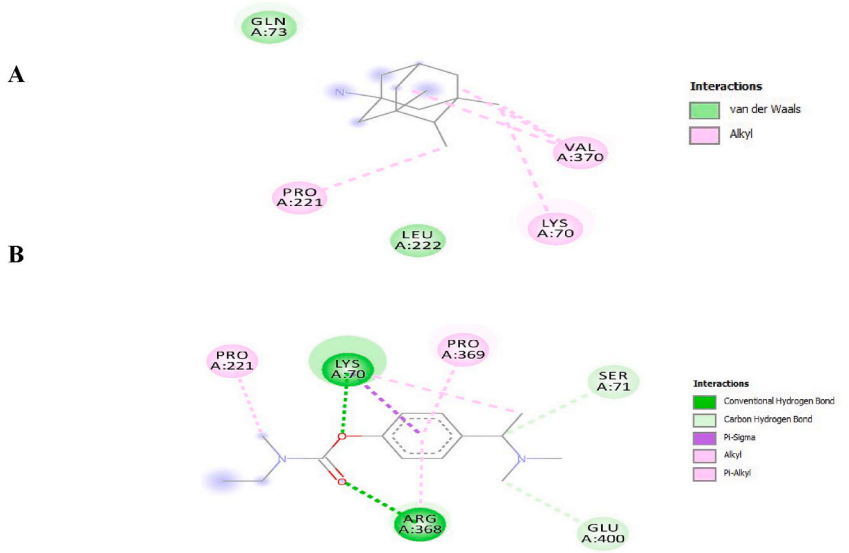

Fig. 5. Two-dimensional representation of the main interactions in the most stable docking states of memantine (**A**) and rivastigmine (**B**) with *beta*-amyloid using Discovery Studio software.

chemical species are more reactive than the harder chemical species [53]. On the other hand, the concept of electron chemical potential (μ), which is often called the electronegativity of a negative atom, is shown as equation (3) [53,55]:

$$\mu = 1 / 2(E_{HOMO} + E_{LUMO}) \quad \text{Eq (3)}$$

Also, the electrophilic index (ω) which indicates the degree of stability of the molecule when receiving electrons, is defined as equation (4) [53,56]:

$$\omega = \mu 2/2\eta \quad \text{Eq (4)}$$

Therefore, the chemical hardness is directly related to the amount of energy gap.

In Table S5, among the two drugs, the chemical hardness of memantine is lower than rivastigmine by 0.02 eV. So, memantine drug is a harder species and this indicates the less activity of this structure. As a result, memantine has a more active structure than rivastigmine.

The value of E_{LUMO} for graphene oxide nanosheet, rivastigmine and memantine is −4.24, −0.14 and −0.22 V, respectively. Also, the values of electrophilic index (ω) for graphene oxide nanosheet is higher than rivastigmine and memantine. Hence, the level energy of graphene oxide is lower than drugs and also due to the higher electrophilic factor of graphene oxide nanosheets than drugs, so it can be said that in the interactions, the direction of electron is from the drug to the graphene oxide nanosheets. It shows a greater affinity to accept electrons from drugs, in which reducing the energy gap and decreases in electrostatic factor occurs through the interaction between the drug and the graphene oxide nanosheet.

The dipole moment is one of the important properties of the molecule, which gives information about the geometric and electronic structure. According to Table S5, the value of dipole moment for memantine is −3.07 and for rivastigmine is −3.05 V.

3.6. Investigation of Mulliken's atomic charges

Mulliken atomic charge distribution was investigated to identify active charge centers in molecules. In the case of rivastigmine, the carbon atom exhibited a maximum positive atomic charge of 1.47 electrons, while the carbon and oxygen atoms had maximum negative atomic charges of 1.026 and 0.809 electrons, respectively. For memantine, the highest positive atomic charges were observed on the carbon and hydrogen atoms, with values of 0.518, 0.578, and 0.215 electrons, while the carbon and nitrogen atoms had corresponding maximum negative atomic charges of 0.643, 0.526, and 0.373 electrons. In graphene oxide, the carbon atoms linked to oxygen had the highest positive atomic charges ranging from 0.788 to 0.600, while the oxygen atoms exhibited the most negative atomic charges ranging from 0.888 to 0.667 electrons. The distribution of positive and negative charges in the molecule is irregular, particularly in the regions containing hydroxy and carbonyl groups. The symmetrical distribution of the Highest Occupied Molecular Orbital (HOMO) and Lowest Unoccupied Molecular Orbital (LUMO) suggests that the absorption energy will be highest when drug molecules are placed near the carbonyl and hydroxy functional groups at the edges of the graphene oxide nanosheet. Memantine has stronger interaction toward graphene oxide nanosheet than rivastigmine. (Fig. S8 and Fig. S9).

3.7. Comparison of molecular docking energy data for memantine and rivastigmine with beta-amyloid protein

By comparing and analyzing the data and energy amounts of memantine and rivastigmine with *beta*-amyloid in the most stable states, are shown in Table 3 and Fig. 5(A and B). The binding energy of the positive control was found to be −8.53 kcal/mol, compared to −9.03 kcal/mol for memantine and −7.81 kcal/mol for rivastigmine, indicating that memantine has a stronger binding affinity.

It can be concluded that:

1) The stability of the complex between memantine and *beta*-amyloid is better than the complex between rivastigmine and *beta*-amyloid due to the lower amount of binding energy
2) The amount of internal energy related to memantine docking with *beta*-amyloid is −9.33 kcal/mol and for rivastigmine is −9.3 kcal/mol, which shows the equality of these two values and this type of energy for both ligands in this position.
3) The sum of van der Waals and hydrogen bond interactions and solvation for memantine with *beta*-amyloid is −7.42 kcal/mol and for rivastigmine with *beta*-amyloid is −8.49 kcal/mol. The results show that the complex of rivastigmine with *beta*-amyloid compared to the complex of memantine with *beta*-amyloid has a lower energy and is more stable.
4) The amount of electrostatic energy for memantine is −1.91 kcal/mol, while for rivastigmine it is −0.81 kcal/mol, which, shows that the complex of memantine and *beta*-amyloid is more stable than the complex of rivastigmine with *beta*-amyloid (Table 3).

Generally, amino acids can form hydrogen bonds due to the presence of carboxylic acid (COOH) and amino groups (NH_2). Memantine forms a hydrogen bond with glutamine, with a bond length of 3.04 A°. Rivastigmine forms stronger hydrogen bonds with lysine and arginine, with bond lengths of 2.96 A° and 2.89 A°, respectively. This suggests that rivastigmine forms stronger hydrogen bonds with *beta*-amyloid compared to memantine. The greater stability and more negative amount of hydrogen bond energy for rivastigmine further support this finding (Fig. 5(A and B) and Fig. 6(A and B)). As shown in Fig. 6, memantine lacks aromatic interactions, while rivastigmine, can engage in aromatic interactions with *beta*-amyloid owing to the presence of an aromatic ring in its structure. In its most stable state (first state), rivastigmine interacts through aromatic interactions with *beta*-amyloid amino acids such as proline (Pro369), arginine (Arg368), and lysine (Lys70). In Fig. 6, the ratio of hydrophobic interactions to hydrogen interactions in the complex of memantine and *beta*-amyloid is equal to 5 to 1, while this ratio for the complex of rivastigmine and *beta*-amyloid is equal to 13 to 2, and it shows that the greater number of interactions is in the complex of rivastigmine and *beta*-amyloid.

Memantine demonstrates more stability compared to rivastigmine-*beta*-amyloid complexes, despite having a greater number and variety of interactions. Factors such as physicochemical properties, structure, spatial orientation, conductivity, and the manner of connection to the desired site should be considered when assessing the stability and effectiveness of a substance or drug. Physicochemical properties, including appearance, boiling point, density, volatility, and solubility in water, can significantly impact the stability and ultimate effectiveness of a drug.

The stability and effectiveness of memantine in *beta*-amyloid complexes can be attributed to its small size, cage-like structure, and the presence of an amin group and alkyl ring. Memantine has a more stable structure with no twists, which contributes to its overall stability and performance in interaction with *beta*-amyloid. On the other hand, rivastigmine is a relatively elongated and large molecule with a flexible structure that may negatively affect its effectiveness and performance in *beta*-amyloid complex. The twists and turns in the structure of rivastigmine can potentially hinder its stability and final effectiveness. In contrast, memantine's stable and rigid structure, along with its specific chemical properties, contribute to its stability and positive effects in *beta*-amyloid complexes (Fig. S10).

3.8. Investiagation of the interaction of rivastigmine and memantine with the graphene oxide sheets

At first, in order to evaluate the interactions between rivastigmine and memantine with graphene oxide nanosheet (Figs. S10a and b), the adsorption energy, enthalpy, and Gibbs free energy, and charge transfer for the complexes of rivastigmine and memantine with graphene oxide nanosheet are reported in **Table 4**.

Based on the results, the interaction between memantine and graphene oxide nanosheet has a more negative adsorption energy (ΔE) (−92.47 kJ/mol) compared to rivastigmine (−86.36 kJ/mol), indicating a stronger attraction. Additionally, the charge transfer (Q) in the memantine-graphene oxide complex (−0.41 kJ/mol) is greater than that of rivastigmine (−0.33 kJ/mol). Also, the negative values of ΔH (−85.71 kJ/mol) and ΔG (−41.52 kJ/mol) propose that the interaction between memantine and graphene oxide is spontaneous. Therefore, it can be concluded that the position of memantine on the graphene oxide sheet provides more suitable conditions for attraction. The charge transfer in both complexes occurs from the HOMO of the drugs to the LUMO of the graphene oxide sheet. The best position for the interaction between the two drugs and the graphene oxide nanosheet is near the hydroxy and carbonyl functional groups. The HOMO electron cloud is focused on the graphene oxide nanosheet, increasing reactivity and absorption energy. The highest absorption energy is observed for memantine. The distribution of molecular orbitals shows that for the caged-like molecule (memantine) the positive electron cloud is spread throughout the structure, indicating better absorption on the nanosheet and a more favorable interaction.

4. Conclusion

This study highlights the potential of memantine and rivastigmine in forming stable complexes with *beta*-amyloid and graphene oxide nanocarriers, which could significantly enhance their therapeutic efficacy for Alzheimer's disease. Memantine, in particular,

Table 3
Comparison of molecular docking energy data of *beta*-amyloid protein with memantine and rivastigmine. The unit of all data is kcal/mol.

Data comparison factors	Memantine	Rivastigmine
Binding-energy	−9.03	−7.81
Ligand-efficiency	−0.64	−0.43
Inhib-constant	239.62	1.89
Intermol-energy	−9.33	−9.3
Vdw-hb-desolve-energy	−7.42	−8.49
Electrostatic-energy	−1.91	−0.81
Total-internal	0.1	−0.42
Torsional-energy	0.3	1.49
Unbound-energy	0.1	−0.42
clRMS	0.01	0.0
refRMS	46.51	44.78

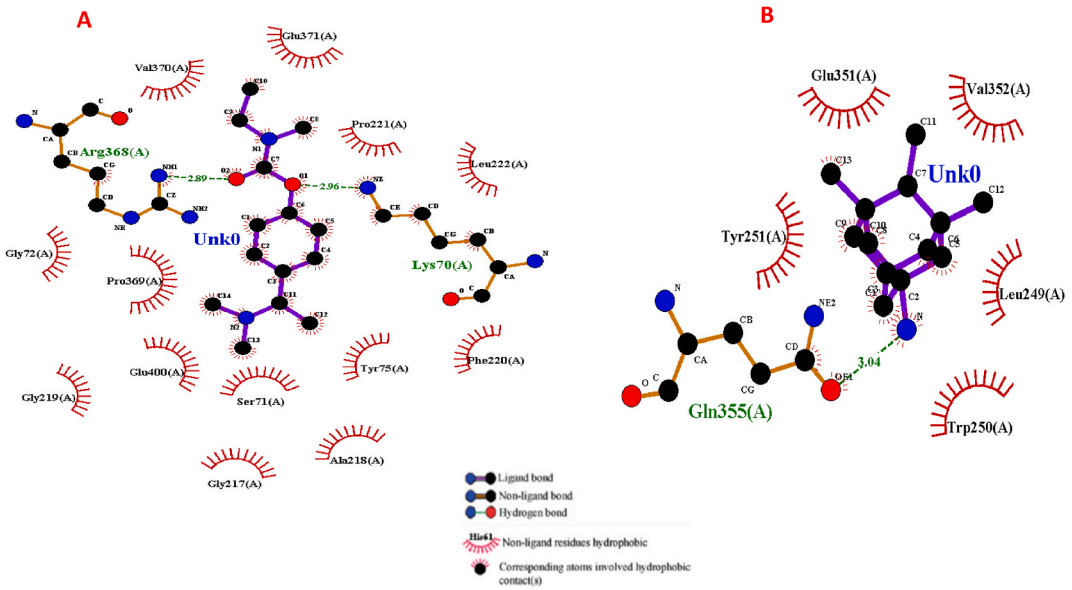

Fig. 6. The number and types of amino acids involved in the interaction of memantine (**A**) and rivastigmine (**B**) with *beta*-amyloid in the most stable states of in Liga-Plot.

Table 4
The interaction energy of memantine and rivastigmine with nanographene oxide nanosheets; Adsorption energy (ΔE), Gibbs free energy (ΔG) and enthalpy (ΔH) in terms of (kJ/mol) and charge transfer (Q).

Complex	ΔE	ΔG	ΔH	Q
Rivastigmine complex	−86.36	−29.27	−77.66	−0.33
Memantine complex	−92.47	−41.52	−85.71	−0.41

shows a more favorable interaction profile, as evidenced by lower binding energy and stronger electrostatic interactions. Molecular docking and in silico results indicate that the binding energies for memantine-beta-amyloid and rivastigmine-beta-amyloid complexes are −9.03 kcal/mol and −7.81 kcal/mol, respectively, suggesting superior stability for the memantine-beta-amyloid complex. The electrostatic energies are −1.91 kcal/mol for memantine and −0.81 kcal/mol for rivastigmine, further supporting the greater stability of the memantine complex. Additionally, memantine's interaction with graphene oxide results in more negative adsorption energy (−92.47 kJ/mol) compared to rivastigmine (−86.36 kJ/mol), indicating a stronger binding affinity. The charge transfer (Q) values are −0.41 kJ/mol for memantine and −0.33 kJ/mol for rivastigmine. The negative enthalpy (ΔH) of −85.71 kJ/mol and Gibbs free energy (ΔG) of −41.52 kJ/mol for the memantine-graphene oxide interaction suggest a spontaneous process. These findings suggest that memantine may be a more effective candidate for further development. Future work should explore the applicability of these findings to other drug classes and natural sources, broadening the scope to include diverse therapeutic agents. Additionally, addressing the limitations of current in silico models and incorporating more comprehensive in vivo studies will be crucial for advancing this research.

CRediT authorship contribution statement

Fateme Davoudi: Writing – original draft, Investigation. **Nasrin Shadjou:** Writing – review & editing, Supervision. **Mahdieh Darroudi:** Writing – original draft, Investigation, Formal analysis, Data curation, Conceptualization.

Declaration of competing interest

The authors declare that they have no known competing financial interests or personal relationships that could have appeared to influence the work reported in this paper.

Acknowledgement

This research was supported by Urmia University. We gratefully acknowledge the support of this work by Urmia University, Urmia, Iran.

Appendix A. Supplementary data

Supplementary data to this article can be found online at https://doi.org/10.1016/j.heliyon.2024.e37702.

References

[1] G. Tosi, F. Pederzoli, D. Belletti, M.A. Vandelli, F. Forni, J.T. Duskey, B. Ruozi, Nanomedicine in Alzheimer's disease: amyloid beta targeting strategy, Prog. Brain Res. 245 (2019) 57–88.
[2] A. Jana, A. Bhattacharjee, S.S. Das, A. Srivastava, A. Choudhury, R. Bhattacharjee, S. De, A. Perveen, D. Iqbal, P.K. Gupta, S. Kumar Jha, S. Ojha, S. Singh, J. Ruokolainen, N.K. Jha, K.K. Kesari, G. Md Ashraf, Molecular insights into therapeutic potentials of hybrid compounds targeting alzheimer's disease, Mol. Neurobiol. 59 (2022) 3512–3528.
[3] H.M. Sosa, R. Keyes, K.A. Stieglitz, Structural analysis of relevant drug targets for Alzheimer's disease: novel approaches to drug development, Curr. Bioact. Compd. 13 (2017) 90–100.
[4] N. Job, V.S. Thimmakondu, K. Thirumoorthy, In silico drug design and analysis of dual amyloid-beta and tau protein-aggregation inhibitors for Alzheimer's disease treatment, Molecules 28 (2023) 1388, 1388.
[5] H. Li, X. Wang, Ho Yu, J. Zhu, H.T. Jin, A. Wang, Z. Yang, Combining in vitro and in silico Approaches to find new candidate drugs targeting the pathological proteins related to the Alzheimer's disease, Curr. Neuropharmacol. 16 (2017) 758–768.
[6] R. Pan, Current drug treatments in Alzheimer's disease, Highlights in Science, Engineering and Technology 36 (2023) 1492–1498.
[7] F. Zhang, R.J. Zhong, R.J. Zhong, C. Cheng, S. Li, W.D. Le, W.D. Le, New therapeutics beyond β-amyloid and tau for the treatment of Alzheimer's disease, Acta Pharmacol. Sin. 42 (2021) 1382–1389.
[8] E. Giacobini, A.C. Cuello, A. Fisher, Reimagining cholinergic therapy for Alzheimer's disease, Brain 145 (2022) 2250–2275.
[9] B.C. Tang, Y.T. Wang, J. Ren, Basic information about memantine and its treatment of Alzheimer's disease and other clinical applications, Ibrain 9 (2023) 340–348.
[10] L.Y. Ivanova, M. Karelson, The impact of software used and the type of target protein on molecular docking accuracy, Molecules 27 (2022) 9041, 9041.
[11] S.K. Nayak, B. Ray, Molecular Docking: Concept and Application, In: Novel Aspects on Pharmaceutical Research 1 (2023) 35–48.
[12] S. Saikia, M. Puzari, P. Chetia, Molecular docking in drug designing and metabolism, Industrial Microbiology and Biotechnology (2023) 403–430.
[13] N. Shadjou, M. Hasanzadeh, Graphene and its nanostructure derivatives for use in bone tissue engineering: recent advances, J. Biomed. Mater. Res. 104 (2016) 1250–1275.
[14] S.N. Abed, P.K. Deb, H.S. Surchi, S.F. Kokaz, S.M. Jamal, S. Bandopadhyay, R.K. Tekade, Nanocarriers in different preclinical and clinical stages, in: In Basic Fundamentals of Drug Delivery, Elsevier, 2019, pp. 685–731.
[15] M. Rezaei Parsafar, Application of nanocarriers in drug delivery and cancer treatment, in: The Fourth International Research Conference in Science and Technology; Saint Petersburg-Russia, 2016.
[16] S. Singh, Nanoparticle based drug delivery system: advantages and applications, Indian J. Sci. Technol. 4 (2011) 177–184.
[17] P. Silva, B. Bonifácio, M. Ramos, K. Negri, T. Maria Bauab, M. Chorilli, Nanotechnology-based drug delivery systems and herbal medicines: a review, Int. J. Nanomed. 1 (2013).
[18] R. Sunasee, C.K. Adokoh, J. Darkwa, R. Narain, Therapeutic potential of carbohydrate-based polymeric and nanoparticle systems, Expert Opin. Drug Deliv. 11 (2014) 867–884.
[19] S. Lorscheidt, A. Lamprecht, Safety assessment of nanoparticles for drug delivery by means of classic in vitro assays and beyond, Expert Opin. Drug Deliv. 13 (2016) 1545–1558.
[20] V. Weissig, D. Guzman-Villanueva, Nanocarrier-based antioxidant therapy: promise or delusion? Expert Opin. Drug Deliv. 12 (2015) 1783–1790.
[21] D.R. Dreyer, S. Park, C.W. Bielawski, R.S. Ruoff, The chemistry of graphene oxide, Chem. Soc. Rev. 39 (2010) 228–240.
[22] T. Szabo, O. Berkesi, P. Forgo, K. Josepovits, Y. Sanakis, D. Petridis, I. Dekany, Evolution of surface functional groups in a series of progressively oxidized graphite oxides, Chem. Mater. 18 (2006) 2740–2749.
[23] Y. Zhu, S. Murali, W. Cai, X. Li, J.W. Suk, J.R. Potts, R.S. Ruoff, Graphene and graphene oxide: synthesis, properties, and applications, Adv. Mater. 22 (2010) 3906–3924.
[24] S. Kim, S. Zhou, Y. Hu, M. Acik, Y.J. Chabal, C. Berger, W. de Heer, A. Bongiorno, E. Riedo, Room-temperature metastability of multilayer graphene oxide films, Nat. Mater. 11 (2012) 544–549.
[25] K.A. Mkhoyan, A.W. Contryman, J. Silcox, D.A. Stewart, G. Eda, C. Mattevi, S. Miller, M. Chhowalla, Atomic and electronic structure of graphene-oxide, Nano Lett. 9 (2009) 1058–1063.
[26] J. Zhao, S. Pei, W. Ren, L. Gao, H.M. Cheng, Efficient preparation of large-area graphene oxide sheets for transparent conductive films, ACS Nano 4 (2010) 5245–5252.
[27] S. Pei, H.M. Cheng, The reduction of graphene oxide, Carbon 50 (2012) 3210–3228.
[28] J.W. Burress, S. Gadipelli, J. Ford, J.M. Simmons, W. Zhou, T. Yildirim, Graphene oxide framework materials: theoretical predictions and experimental results, Angew. Chem. Int. Ed. 49 (2010) 8902–8904.

[29] C. Gómez-Navarro, R.T. Weitz, A.M. Bittner, M. Scolari, A. Mews, M. Burghard, K. Kern, Electronic transport properties of individual chemically reduced graphene oxide sheets, Nano Lett. 7 (2007) 3499–3503.

[30] X.Y. Meng, H.X. Zhang, M. Mezei, M. Cui, Molecular docking: a powerful approach for structure-based drug discovery, Curr. Comput. Aided Drug Des. 7 (2011) 146–157.

[31] M. Inagaki, F. Kang, Engineering and applications of carbon materials, in: In Materials Science and Engineering of Carbon: Fundamentals, Elsevier, 2014, pp. 219–525.

[32] P.T. Phanrang, I.R. Singh, A.K. Chandra, S. Mitra, Molecular insights on the modulated acetylcholinesterase inhibition activity of tacrine adsorbed on biocompatible graphene oxide, ChemistrySelect 8 (2023).

[33] F.S. Alhodieb, M.A. Rahman, M.A. Barkat, A.A. Alanezi, H.A. Barkat, H.A. Hadi, R.K. Harwansh, V. Mittal, Nanomedicine-driven therapeutic interventions of autophagy and stem cells in the management of Alzheimer's disease, Nanomedicine 18 (2023) 145–168.

[34] M.J. Frisch, G.W. Trucks, H.B. Schlegel, G.E. Scuseria, M.A. Robb, J.R. Cheeseman, G. Scalmani, V. Barone, G.A. Petersson, H. Nakatsuji, X. Li, M. Caricato, A. V. Marenich, J. Bloino, B.G. Janesko, R. Gomperts, B. Mennucci, H.P. Hratchian, J.V. Ortiz, A.F. Izmaylov, J.L. Sonnenberg, D. Williams-Young, F. Ding, F. Lipparini, F. Egidi, J. Goings, B. Peng, A. Petrone, T. Henderson, D. Ranasinghe, V.G. Zakrzewski, J. Gao, N. Rega, G. Zheng, W. Liang, M. Hada, M. Ehara, K. Toyota, R. Fukuda, J. Hasegawa, M. Ishida, T. Nakajima, Y. Honda, O. Kitao, H. Nakai, T. Vreven, K. Throssell, J.A. Montgomery Jr., J.E. Peralta, F. Ogliaro, M.J. Bearpark, J.J. Heyd, E.N. Brothers, K.N. Kudin, V.N. Staroverov, T.A. Keith, R. Kobayashi, J. Normand, K. Raghavachari, A.P. Rendell, J.C. Burant, S. S. Iyengar, J. Tomasi, M. Cossi, J.M. Millam, M. Klene, C. Adamo, R. Cammi, J.W. Ochterski, R.L. Martin, K. Morokuma, O. Farkas, J.B. Foresman, D.J. Fox, Gaussian 06, Revision D. 01, vol. 620, Gaussian, Inc., Wallingford CT, 2009. See also: URL: http://www.gaussian.com.

[35] M.J. Frisch, G.W. Trucks, H.B. Schlegel, G.E. Scuseria, M.A. Robb, J.R. Cheeseman, G. Scalmani, V. Barone, B. Mennucci, G.A. Petersson, H. Nakatsuji, M. Caricato, X. Li, H.P. Hratchian, A.F. Izmaylov, J. Bloino, G. Zheng, J.L. Sonnenberg, M. Hada, M. Ehara, K. Toyota, R. Fukuda, J. Hasegawa, M. Ishida, T. Nakajima, Y. Honda, O. Kitao, H. Nakai, T. Vreven, J.A. Montgomery Jr., J.E. Peralta, F. Ogliaro, M. Bearpark, J.J. Heyd, E. Brothers, K.N. Kudin, V. N. Staroverov, R. Kobayashi, J. Normand, K. Raghavachari, A. Rendell, J.C. Burant, S.S. Iyengar, J. Tomasi, M. Cossi, N. Rega, J.M. Millam, M. Klene, J.E. Knox, J.B. Cross, V. Bakken, C. Adamo, J. Jaramillo, R. Gomperts, R.E. Stratmann, O. Yazyev, A.J. Austin, R. Cammi, C. Pomelli, J.W. Ochterski, R.L. Martin, K. Morokuma, V.G. Zakrzewski, G.A. Voth, P. Salvador, J.J. Dannenberg, S. Dapprich, A.D. Daniels, O. Farkas, J.B. Foresman, J.V. Ortiz, J. Cioslowski, D.J. Fox, GAUSSIAN 09 (Revision A.02), Gaussian, Inc., Wallingford, CT, 2009.

[36] G.M. Morris, R. Huey, W. Lindstrom, M.F. Sanner, R.K. Belew, et al., AutoDock4 and AutoDockTools4: automated docking with selective receptor flexibility, J. Comput. Chem. 30 (2009) 2785–2791, https://doi.org/10.1002/jcc.21256.

[37] G.M. Morris, R. Huey, W. Lindstrom, M.F. Sanner, R.K. Belew, D.S. Goodsell, A.J. Olson, AutoDock4 and AutoDockTools4: automated docking with selective receptor flexibility, J. Comput. Chem. 30 (2009) 2785–2791.

[38] D.S. Biovia, Discovery Studio Modeling Environment. Release, 2017.

[39] J.D. Chai, Mead-Gordon, Long-range corrected hybrid density functionals with damped atom-atom dispersion corrections, Phys. Chem. Chem. Phys. 10 (2008) 6615–6620.

[40] A.D. Becke, Density-functional thermochemistry. I. The effect of the exchange-only gradient correction, J. Chem. Phys. 96 (1992) 2155–2160.

[41] V. Purghasem, Docking Studies on Interaction of Taxol Derivatives with SS-Tubulin to Introduce More Effective Anticancer Drug, Master's Thesis Shahid Beheshti University Faculty of Chemistry, 2014.

[42] H. Mehmood, M. Haroon, T. Akhtar, S. Woodward, S. Haq, Synthesis, anti-diabetic profiling and molecular docking studies of 2-(2-arylidenehydrazinyl) thiazol-4(5H)-ones, Future Med. Chem. 16 (2024) 1255–1266.

[43] H. Mehmood, T. Akhtar, M. Haroon, M. Shah, U. Rashid, S. Woodward, Synthesis of hydrazinylthiazole carboxylates: a mechanistic approach for treatment of diabetes and its complications, Future Med. Chem. 15 (2023) 1149–1165.

[44] Y. Iqbal, T. Akhtar, M. Haroon, H. Mehmood, T. Nizami, M. Ehsan, 4-Adamantyl-(2-(arylidene) hydrazinyl) thiazoles as potential antidiabetic agents: experimental and docking studies, Future Med. Chem. 15 (2023) 599–613.

[45] M. Haroon, M. Khalid, K. Shahzadi, T. Akhtar, S. Saba, J. Rafique, S. Ali, M. Irfan, M. Alam, M. Imran, Alkyl 2-(2-(arylidene) alkylhydrazinyl) thiazole-4-carboxylates: synthesis, acetyl cholinesterase inhibition and docking studies, J. Mol. Struct. 1245 (2021) 131063.

[46] S. K, M. Haroon, M. Khalid, T. Akhtar, T. Ghous, M. Alam, M. Imran, Synthesis and in silico docking studies of ethyl 2-(2-Arylidene-1-alkylhydrazinyl)thiazole-4-carboxylates as antiglycating agents, Chem. Biodivers. 19 (2022) e202100581.

[47] M. H, T. Akhtar, M. Haroon, E. Tahir, M. Ehsan, S. Woodward, M. Musa, Synthesis of arylidenehydrazinyl-4-methoxyphenylthiazole derivatives: docking studies, probing type II diabetes complication management agents, Chem. Biodivers. 19 (2022) e202200824.

[48] I. H, T. Akhtar, A. Aktaş, E. Tahir, M. Ehsan, Synthesis of thiazole-chalcone hybrid molecules: antioxidant, alpha(α)-amylase inhibition and docking studies, Chem. Biodivers. 20 (2023) e202201134.

[49] M. H, T. Akhtar, M. Haroon, M. Khalid, S. Woodward, M. Asghar, R. Baby, R. Orfali, R. Perveen, Synthesis of fluorinated hydrazinylthiazole derivatives: a virtual and experimental approach to diabetes management, ACS Omega 8 (2023) 11433–11446.

[50] H. M., M. Haroon, T. Akhtar, S. Woodward, H. Andleeb, Synthesis and molecular docking studies of 5-acetyl-2-(arylidenehydrazin-1-yl)-4-methyl-1,3-thiazoles as α-amylase inhibitors, J. Mol. Struct. 1250 (2022) 131807.

[51] M. Mohamad, Modelling and Simulation of Structural, Electronic and Optical Properties of Organic Semiconducting Materials, Faculty of Science, Universiti Teknologi Malaysia, 2017. PhD thesis.

[52] T. Moeller, J.C. Bailar, J. Kleinberg, C.O. Guss, M.E. Castellion, C. Metz, Periodic Perspective: the Representative Elements, 1980, pp. 273–298.

[53] M. Darroudi, Theoretical and experimental study of ring addition reactions of acetylene derivatives for the synthesis of heterocyclic compounds such as *β*-octams. Chromenes and Triazoles/PhD Thesis in the Field of Organic Chemistry/Faculty of Chemist, Mazandaran University, Sari-Iran, 2017.

[54] L.R. Domingo, A density functional theory study for the diels-alder reaction between N-Acyl-1-Aza-1,3-Butadienes and vinylamines. Lewis acid catalyst and solvent effects, Tetrahedron 58 (2002) 3765–3774.

[55] A. Arrieta, D. Otaegui, A. Zubia, F.P. Cassio, A. Díaz-Ortiz, A. de la Hoz, M.A. Herrero, P. Prieto, C. Foces-Foces, J.L. Pizarro, M.I. Arriortua, Solvent-free thermal and microwave-assisted [3+2] cycloadditions between stabilized azomethine ylides and nitrostyrenes. An experimental and theoretical study, J. Org. Chem. 72 (2007) 4313–4322.

[56] V. Bénéteau, A. Olmos, T. Boningari, J. Sommer, P. Pale, Zeo-click synthesis: CuI-Zeolite-Catalyzed one-pot two-step synthesis of triazoles from halides and related compounds, Tetrahedron Lett. 51 (2010) 3673–3677.